# Actuated Bistable Jumping Structures

**Matthew Santer**
Department of Aeronautics,
Imperial College London,
Prince Consort Road,
London SW7 2AZ, UK
e-mail: m.santer@imperial.ac.uk

*The design and analysis of a fully actuated adaptive bistable structure is presented. This structure releases energy at a high frequency, which in consequence causes it to jump. Such structures have application as the basis for multistable adaptive systems. The dynamic transition of the bistable structure from its high-energy to low-energy stable states and the lower-frequency return transition are considered by reference to a specific example. The effect of embedded actuation on this behavior is also investigated.*
[DOI: 10.1115/1.4000417]

## 1 Introduction

Bistable structures have great potential for use in adaptive systems and may be used as building blocks for multistable structures with very large numbers of discrete stable configurations [1]. Bistable structures have two discrete stable configurations. The transition between these states may require a large geometric shape change. In particular, this change in form through structural compliance, without the requirement for conventional mechanism components, makes them attractive for use in adaptive systems, especially in environments that are not well suited to conventional mechanisms [2]. Possible applications also include switches and valves both at microscale [3] and macroscale. It is also worth noting that examples of actuated bistable structures may be found in the natural world, for example the Venus fly-trap [4].

It has previously been shown that bistable structures may store equal amounts of strain energy in their two stable configurations [5]. These are termed symmetrically bistable structures. Such structures are useful for applications in which each stable state is of equal importance. Bistable structures, which have one stable state that is energetically preferential to the other—asymmetrically bistable structures—may be beneficial when there is a requirement for work to be done by the structure [6]. The strain energy difference between the stable states may be converted to work during the transition between the high-energy state and the low-energy state at a higher frequency than achievable with current large stroke actuators. This unilateral high-frequency transition between stable states of an asymmetrically bistable structure is the predominant focus of this paper.

A corollary of this release of strain energy as work during the transition from the high-to low-energy states is, of course, that this energy must be input by the actuators effecting the transition in the opposite direction. Consequently, the return transition must take place at a significantly lower frequency as energy is pumped into the system with a substantially greater burden placed on the actuators. The presence of return actuators can significantly effect the properties of the high-frequency transition. One possible application for bistable structures is in morphing aircraft concepts [7] and the ability to actuate them repeatedly between the stable states is essential if they are to be used in real systems

It is necessary, if such bistable structures are to be used in adaptive systems, to be able to predict their performance with confidence. To date, this prediction has largely focused on the stable equilibrium configurations [6]. The steady-state geometric configurations are essential to determine the forms that a multistable system constructed from bistable elements will adopt and it is not necessary for this to consider the dynamics of the transition. Indeed in a finite element analysis (FEA) it is often convenient to change the geometric configuration by means of a displacement-controlled approach to assist convergence.

In conceivable physical implementations of multistable systems based on actuated bistable units, however, the change in configuration is force-controlled and the dynamics of the transition must be accounted for. This is particularly important for two reasons. The first is that it is necessary to know the effect of the actuation of a single bistable unit on the remainder of the structure. The transmission of vibration due to high-frequency dynamic snap-through could be critical, for example, in a space-based optical system. The second is that the dynamics of the transition between stable states can significantly affect the efficiency of energy transfer with more or less being converted to internal kinetic energy instead of work.

In this paper, analysis of the transitions between the stable states of an asymmetrically bistable structure will be developed and demonstrated. The structure that will be demonstrated manifests the release of stored strain energy as useful work by jumping, providing a graphical illustration of the effect. It will be shown how currently available actuator technology can be used to actuate the transitions in both directions—this is essential if bistable elements are to be used in functional multistable systems.

Following this introduction, the concept of asymmetric bistability will be introduced. A specific example of an actuated asymmetrically bistable structure will be shown, which will be used to demonstrate the developed analysis techniques. These techniques, which increase in complexity from the assumption of perfect energy transfer to a nonlinear dynamic finite element analysis, demonstrate the behavior of the specific structure and also enable more general conclusions concerning the design and actuation of bistable structures to be made.

## 2 Concept

**2.1 Asymmetric-Bistability.** An asymmetrically bistable structure may be generated by coupling a spring with a linear response and a spring with a nonlinear response. This technique has been previously demonstrated through the design of triangulated bistable structural elements [6]. Therefore, this technique is also used to generate the jumping structures analyzed in this paper. The nonlinear springs that are used are tape springs, which exert an approximately linear moment under an increasing applied end rotation until a limit point is reached at a critical moment $M_{\text{lock}}$ and the structure buckles. Under continued end rotation the tape spring regains stability (positive stiffness) but exerts a smaller and approximately constant moment $M^*$ [8].

When a tape spring is conceptually coupled with a leaf spring—which exhibits a linearly increasing moment when subject to an increasing applied end rotation—the rotation-moment curves of the two springs intersect at three points, which correspond to equilibrium configurations. This coupling is illustrated in Fig. 1(*a*) in

Contributed by the Applied Mechanics Division of ASME for publication in the JOURNAL OF APPLIED MECHANICS. Manuscript received October 9, 2008; final manuscript received August 14, 2009; published online February 8, 2010. Assoc. Editor: N. Sri Namachchivaya.

  

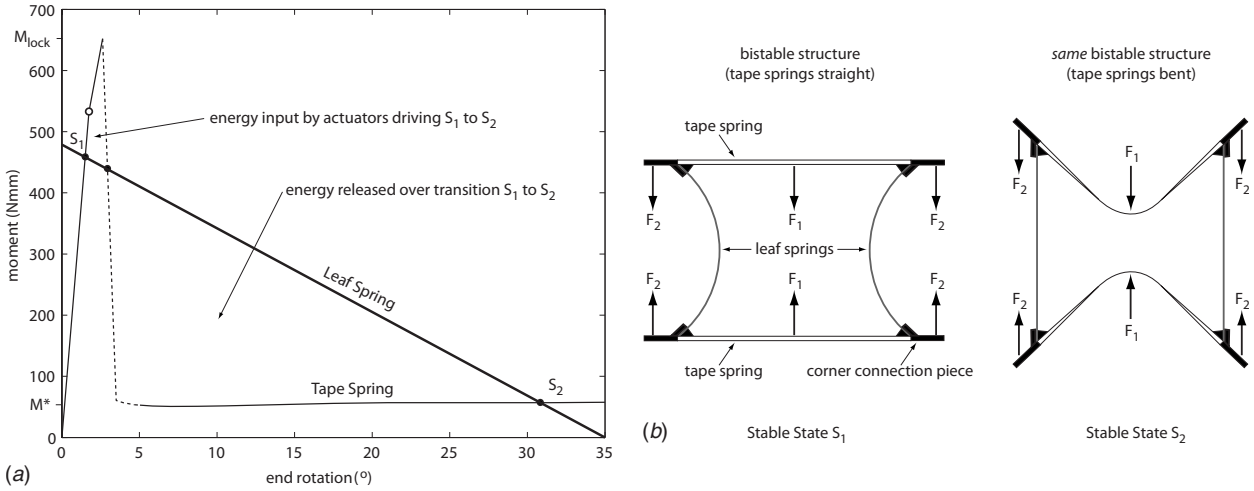


**Fig. 1 (*a*) Graph showing moment versus rotation for a paired tape spring and leaf spring and (*b*) jumping bistable structure concept, showing both stable states.**

which the leaf spring response is represented by a thick line, and the tape spring response by a thin line. Where the line is dotted corresponds to an unstable configuration. The three equilibrium configurations where the lines intersect are highlighted with black dots. The properties of the tape spring and leaf spring used to create the figure are those of the design elaborated in Sec. 3.

It can be seen that two of these equilibrium configurations are stable, which occurs when both the leaf spring and the tape spring have positive stiffness at the intersection of their equilibrium curves. These are when the tape spring is straight and the leaf spring bent at point $S_1$ and vice-versa at point $S_2$. The strain energy is represented in the graph by the areas bounded by the curves. It can be seen that the stored energy that is released at high frequency during the transition from the high-to the low-energy stable state, and which may be converted to work, is considerably greater than the energy required to move the configuration from $S_1$ to the unstable equilibrium point after which it will jump to $S_2$ of its own accord.

**2.2 Actuated Jumping Structure.** Using the concept for generating asymmetrically bistable structures described in the previous section, a design for a bistable structure having two tape springs and two leaf springs was developed. This design is illustrated in Fig. 1(*b*). The moment-rotation relationships at each of the four points at the corners where the tape springs are connected to the leaf springs are represented by the graph in Fig. 1(*a*). The structure is illustrated in the two stable equilibrium configurations $S_1$ and $S_2$. A physical realization of the concept requires a method of attaching the spring elements to each other. This is carried out by rigid connection pieces, which are shown shaded black in the figure. These corner connection pieces also serve two auxiliary functions, in that they provide an attachment point for resetting actuators and also feet to enable the structure to jump when the high-frequency transition occurs.

The actuation scheme adopted is represented by the forces shown in Fig. 1(*b*). In this scheme a single actuator driving the transition from $S_1$ to $S_2$ is opposed by two actuators to carry out the more difficult translation in the return direction. The first actuator is represented by the force $F_1$, which is applied transversely to the tape springs at their midpoint. Their role is to break the spines of the tape springs by imparting a moment greater than $M_{\text{lock}}$. At this point the high-frequency transition to the low-energy stable state begins, causing the leaf springs to straighten.

The two opposing actuators, which are represented by the force $F_2$ are offset from the spring ends by means of the rigid corner connection pieces. Their role is to bend the leaf springs by imparting an end moment, restoring the strain energy that was released during the transition in the opposite direction to the unstable equilibrium configuration at which point the structure will jump to its original stable equilibrium configuration $S_1$.

The ideal actuators employed in this scheme exert zero force when they are not carrying out their assigned roles. The majority of available actuation technologies, however, is not unilateral and exerts force even when they are not in use. In consequence all actuators can have an effect on the transition between the stable equilibrium configurations in both directions. In the structure that is analyzed below, for example, the nonzero restoring force $F_1$ during the low-to-high energy transition $S_2$ to $S_1$ has significant implications on the required performance of the actuators providing force $F_2$.

It should be mentioned that the structural concept shown in Fig. 1(*b*) has two conceivable additional stable equilibrium configurations in which only one of the tape springs is bent while the other remains straight. These configurations may be avoided by ensuring designs in which the moment exerted by the leaf springs on the straight tape spring when the other tape spring is bent is greater than $M_{\text{lock}}$.

## 3 Design and Analysis

The specific design of actuated asymmetrically bistable structure of the form shown in Fig. 1(*b*) used to demonstrate the analysis techniques and structural performance in this paper is now introduced. Both the tape springs and leaf springs are spring steel with a Young's modulus $E$ of 210 GPa, Poisson's ratio $\nu$ of 0.3, and density $\rho$ of 7900 $\text{kg/m}^3$. The lengths of the leaf springs $a$ and the length of the tape springs $b$ are both 120 mm. The leaf springs have a thickness of 0.52 mm and a depth of 19.05 mm. The bending stiffness of a single leaf spring $EI$ is therefore $47{,}000\ \text{N mm}^2$. The tape springs have a cross section with a circular arc of circumferential length 25.4 mm and a radius of curvature 12.6 mm and subtending an angle of 75.0 deg.

The tape springs and leaf springs are connected by wire-cut Aluminum alloy corner pieces, which are assumed to be rigid in all subsequent analyses. They provide an attachment to ensure that the tape springs and leaf springs meet at the correct angle $\alpha$, which is fixed at 55.0 deg. In addition, they provide an attachment point for the actuators driving the $S_2$ to $S_1$ transition offset from the corner by 17.0 mm. A jumping foot of length 25.0 mm is also incorporated. The total mass of the bistable structure including three spring actuators of the type described below is 70 g.

**3.1 Equilibrium Configurations.** The graph plotted in Fig. 1(*a*) shows the conceptual response of a single paired tape spring

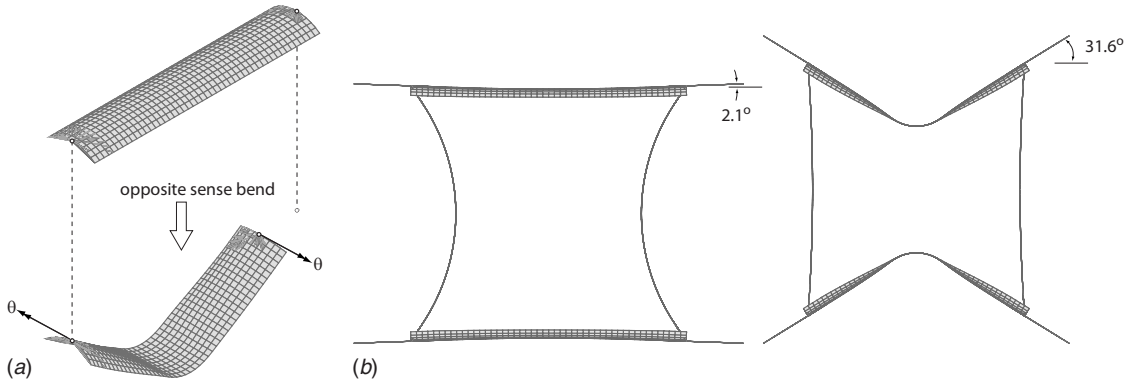


**Fig. 2** (*a*) **FEA of a tape spring in opposite-sense bending and** (*b*) **FEA of the bistable structure showing the stable equilibria when** $F_2=0$

and leaf spring having these geometries and properties. It should be noted that the tape spring is subject to opposite-sense bending, meaning that the applied curvature along the length is defined in the opposite direction to the curvature of the cross section [8]. The tape spring properties were evaluated using the commercial finite element software SAMCEF [9,10]. The tapes springs are modeled with four-node quadratic Mindlin shell elements, with a master node at the center of each end. There are ten elements along the cross section and 48 along the length. All nodes associated with the first and last four rows of elements along the length are fixed to the nearest master node with rigid elements. This level of discretization has been shown to capture the bending behavior of tape springs adequately [11]. The master node at one end is constrained against all translational motion. The other master node is constrained against two translations but is free to translate in the direction of the original tape spring axis. Opposite sense end rotation is applied at both master nodes up to a value of 35.0 deg as shown in Fig. 2(*a*). A Newton–Raphson iterative process with adaptive time-stepping is adopted.

It can be seen from Fig. 1(*a*) that the tape spring exerts a maximum moment in bending of approximately 650 N mm and an approximately constant post-buckled moment of 50 N mm. The geometry of the leaf spring provides a suitable margin of safety between $S_1$ and the first onset of buckling—marked with a white dot in the figure. It is of interest to confirm that the graph in Fig. 1(*a*) for a single paired tape spring and leaf spring is applicable to predict the stable states when two tape springs and leaf springs are paired. This is carried out by means of a geometrically nonlinear FEA in SAMCEF.

As the asymmetrically bistable structure requires the connection of tape springs that are prestressed and deformed with undeformed leaf springs, the finite element model is assembled in a two-stage process. In the first stage the tape springs, modeled as described above, are separated vertically by the undeformed length of the leaf springs. The leaf springs, like the tape springs, are modeled with four-node quadrilateral Mindlin shell elements, with ten elements along the cross section and 48 elements along the length. The master nodes, colocated with the master nodes for the tape springs, are defined at the ends of the leaf springs, which are then connected to the nearest nodes associated with the first and last 4 rows of elements along the leaf spring length.

The four pairs of colocated master nodes are connected with a mechanical hinge element, which ensures that the colocation is retained but permits relative rotation about the end rotation axis. The ends of both tape springs are then rotated by the desired amount. Because of the hinged connection the leaf springs ends remain colocated without the leaf springs deforming. When the desired tape spring end rotation is achieved, the relative end rotations of the tape and leaf springs are then fixed. At this point all prescribed displacements are removed and the structure relaxes into its low-energy stable configuration. This configuration is shown on the right hand side of Fig. 2(*b*).

In order to determine the high-energy stable configuration, end rotations are applied to the tape springs to straighten them. As the relative rotation to the leaf springs is now fixed, the leaf springs are now deformed by this action. When the tape springs are straight, the prescribed displacements are removed and the structure relaxes into its high-energy stable configuration. This configuration is shown on the left hand side of Fig. 2(*b*). A similar process may be used to verify that, for the chosen design, there are no additional stable configurations with one tape spring bent and the other straight. If the structure is deformed to one of these configurations, in each case the structure relaxes to the low-energy stable state already determined.

It should be noted that the stable configurations shown in Fig. 2(*b*) correspond extremely well to the rotations predicted by the simple analysis shown in Fig. 1(*a*). Although not shown here, the same sequence of analyses confirmed that when the actuation forces $F_1$ and $F_2$ were included, as defined below for the shape memory alloy spring actuators, similar stable equilibrium configurations of the bistable structure were determined to exist. Finally, the stable equilibrium configurations were confirmed by the behavior of the physical model described in Sec. 4.2.

**3.2 Actuator Functional Modeling.** In addition to the equilibrium analysis described above, in order to capture the behavior of the transitions it is necessary to have a functional representation of the actuator force at a given displacement. The choice of actuator is clearly dependent on the requirements of the bistable structure and, in the case when the actuator force is nonzero when it is not driving a transition, can itself have a significant effect on the transition behavior. The selection of a suitable actuator and bistable structure design is therefore an iterative process.

In general the actuation requirements for bistable structures that undergo large geometric changes between their stable states are that they have a high stroke and a moderate blocked force. Frequency requirements are low, particularly in the case of the structures presented in this paper in which high-frequency behavior arises from the structure itself. Many other useful actuator metrics have been determined elsewhere [12]. Various suitable actuation options exist, including amplified piezoelectric stacks, and the novel technology of nematic elastomers [13]. Here, however, the actuators that are used are Nickel-Titanium (NiTi) shape memory alloy (SMA) springs. These are described in greater detail below. The same process adopted for modeling the incorporation of SMA springs into the bistable structure transition analysis may be used for any actuator technology.

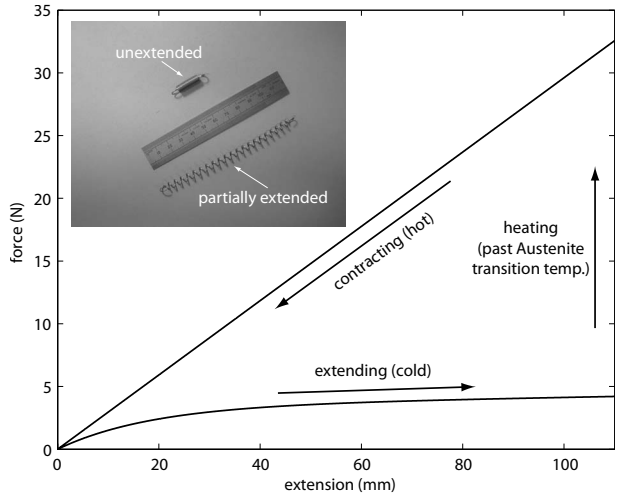


**Fig. 3 Functional representation of a full actuation cycle of a NiTi spring actuator (shown in the inset)**

The commercially available NiTi tension spring actuator used[1] is pictured in the inset to Fig. 3. Its unstretched length $L_0$ is 28 mm, and it is rated with a free stroke of 110 mm and a blocked force of greater than 30 N. This is shown to be compatible with the chosen bistable structure geometry actuated according to the scheme shown in Fig. 1(*b*). In order to determine a representative function, quasistatic tensile tests were carried out using an Instron 5567 materials testing machine. The cold spring was extended by 110 mm at a rate of 0.02 mm/s and the force recorded. The functional representation of this cold extensional behavior, superimposed on the experimental data are plotted in Fig. 3. It can be seen that the extensional behavior consists of a linear component, which results from the helical spring geometry, and a nonlinear component exhibiting an initial large increase in force with extension followed by a plateau, which results from the plasticlike martensitic transformation of the SMA.

In order to measure the actuation properties of the NiTi spring, it was heated past the SMA austenite transition temperature by passing a current of 2 A through the wire. With the spring being maintained in its heated configuration, the end extension was reduced to zero at a rate of 0.02 mm/s and the corresponding force recorded. The functional representation of this hot actuation superimposed on the experimental data is shown in Fig. 3. It can be seen that the heated NiTi spring actuator behaves as a linear spring that exerts substantially more force than is required to extend it in its cold martensite state.

The functional representation was carried out with reference to the observed form of the response. The chosen function was fitted to the experimental data using a least-squares analysis within MATLAB [14]. The linear functional representation of force $F_{\text{hot}}$ N versus extension $x$ mm of the hot contraction was found by this approach to be

$$F_{\text{hot}} = 0.296x \tag{1}$$

The cold extension of the NiTi spring was represented by a constant and an exponentially decaying term. The functional representation of force $F_{\text{cold}}$ N versus extension $x$ mm of the cold extension was found by this approach to be

$$F_{\text{cold}} = 3.419(1 - \exp(-0.054x)) + 0.0072x \tag{2}$$

These expressions are substituted for $F_1$ and $F_2$ in the analyses below depending on whether the actuator is driving a transition (hot) or in opposition to the transition (cold).

[1]http://www.robotstore.com

**3.3 Upper Bound Energy-Based Analysis.** The transfer of stored strain energy in an asymmetrically bistable structure to useful work—in the case of the jumping structures presented here resulting in an increase in potential energy—during the transition from $S_1$ to $S_2$ is one of the primary focuses of this paper. It is therefore worthwhile to provide a simple upper bound calculation of the maximum jump height that can be attained if energy is perfectly transferred, which may then be used to assess the efficiency of the actual energy transfer that is attained. Clearly this approach can give no information concerning the frequency of the transition.

For the jumping bistable structure described above, it is necessary to account for the energy required to extend the actuators $F_2$ over the transition. The energy input by the driving actuator $F_1$ is, however, neglected as once the unstable equilibrium point is traversed, the energy transfer occurs at a much higher frequency than the operation of the actuator. Physically this means that, as dynamic snap-through occurs the folds of the tape springs come closer together faster than the actuator contracts, and the actuator is therefore pushed to one side.

In this and the following analysis, two cases are considered. One considers the full functional representation of the actuators as defined in Eqs. (1) and (2). The other assumes that $F_{\text{cold}}=0$, which is representative of the performance that could be attained if unilateral actuators were used. The mass of the actuators is still included in the potential energy estimate. The jump height evaluated by this energy approach $s_{\text{en}}$ attained by the bistable structure is

$$s_{\text{en}} = \frac{(U_\epsilon - U_{\text{act}})}{mg} \tag{3}$$

in which $U_\epsilon$ is the strain energy released by the structure over the transition, as shown in Fig. 1(*a*), $U_{\text{act}}$ is the energy required to extend opposing actuators, $m$ is the mass of the structure, and $g$ is the acceleration due to gravity.

**3.4 Simplified Analytical Model.** In order to obtain an improved estimate of the jump height—illustrative of the efficiency of energy transfer—and also to obtain a first estimate of snap-through frequency, a dynamic analysis of the $S_1$ to $S_2$ transition based on a simplified model is now considered. This simplified model is a pseudorigid-body model of the type introduced by Howell [2]. One-half of the simplified structure is considered by means of a symmetry argument. A sketch of the model in its low-energy equilibrium configuration $S_2$, which defines the notation used and the associated free body diagram is shown in Fig. 4. The same geometry and notation is also adopted for the quasistatic reset analysis below.

In the figure, the tape springs are idealized as pinned rigid members that exert a constant restoring moment $M^*$. The geometry of the structure at any moment in time is assumed to be uniquely defined by the counterclockwise positive rotation $\psi$ of the top corner. The equilibrium configuration $S_2$ occurs when both corners are rotated by an angle $\psi_{\text{eq}}$ from the horizontal. For this single degree of freedom model to be correct it is necessary to assume a shape for the leaf spring (shown gray) that is fully parameterized by $\psi$. The shape adopted is a circular arc with curvature $\kappa(\psi)$. The leaf spring exerts a restoring moment $M_{\text{ls}}=EI\kappa$. The assumption of a transition path, which is symmetrical about both center lines, and which is identical for both reset and dynamic transitions is necessary to make the analysis tractable but is not necessarily representative of the actual behavior.

Rigid pieces at the corners provide an attachment offset $L_1$ for the actuators represented by the force $F_2$, and a jumping foot of length $L_2$. The mass $m$ in this simplified dynamic analysis is equal to one quarter of the total structural mass. In the dynamic model, the motion during the transition is expressed in terms of the vertical displacement of the top and bottom corners $x_t$ and $x_b$, respectively, and by the horizontal displacement $y$, which is the same for both corners. The instantaneous extensions of the actuators repre-

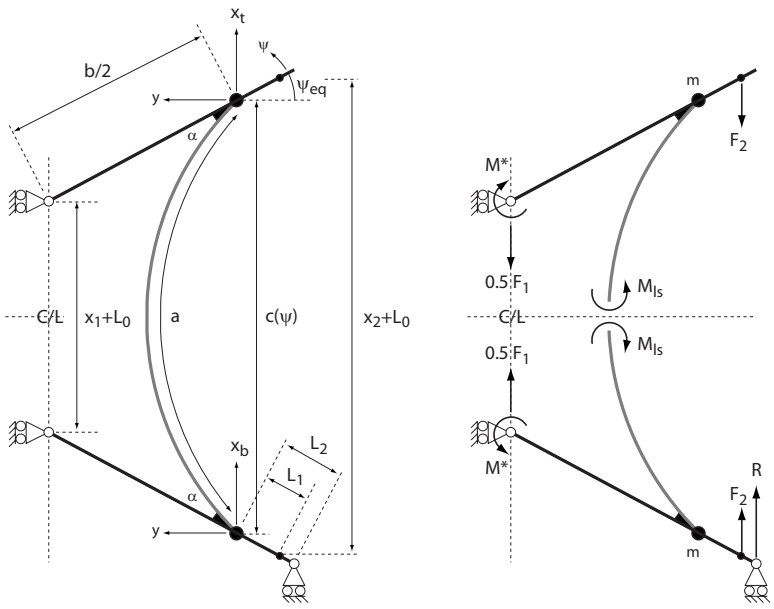


**Fig. 4 Simplified dynamic model and associated free body diagram of the bistable jumping structure**

sented by the forces $F_1$ and $F_2$ are $x_1$ and $x_2$, respectively. The arrows in the figure denote positive displacement. The vertical force $R$ exerted by the jumping foot enables the time of the jump and the height to be determined. It should be noted that the horizontal reaction forces at the supports on the vertical axis of symmetry are not drawn as they have zero value for the assumed transition path.

The conservation of energy in the structure, in which the energy due to accelerating the masses and inertias is incorporated in the D'Alembert sense, over an infinitesimal change in configuration may be expressed as

$$m(\ddot{x}_b dx_b + \ddot{x}_t dx_t + 2\ddot{y}dy) + F_1 dx_1 + 2F_2 dx_2 + 2(M^* - M_{ls})d\psi = 0 \tag{4}$$

As the model is fully defined by the rotation angle $\psi$ it is possible to express Eq. (4) uniquely in terms of this variable. It may readily be shown that

$$\ddot{x}_b = \frac{dx_b}{d\psi}\ddot{\psi} + \frac{d^2x_b}{d\psi^2}\dot{\psi}^2 \tag{5}$$

and similarly for $x_t$ and $y$. $F_1$ is zero throughout the high-frequency transition for the reasons discussed above and $F_2(x_2)$ may be determined by means of Eq. (2). The actuator extensions are expressed as

$$x_1 = c(\psi) - b\,\sin(\psi_{eq} + \psi) - L_0 \tag{6}$$

$$x_2 = c(\psi) + 2L_1\,\sin(\psi_{eq} + \psi) - L_0 \tag{7}$$

in which the abbreviated geometric variable

$$c(\psi) = \frac{2a}{(\pi - 2\alpha - 2(\psi_{eq} + \psi))}\sin\left(\frac{\pi - 2\alpha - 2(\psi_{eq} + \psi)}{2}\right) \tag{8}$$

The corner displacements are expressed in terms of $\psi$ as

$$x_b = L_2(\sin(\psi_{eq} + \psi) - \sin\,\psi_{eq}) \tag{9}$$

$$x_t = L_2(\sin(\psi_{eq} + \psi) - \sin\,\psi_{eq}) + c(\psi) - c(0) \tag{10}$$

$$y = \frac{b}{2}(\cos\,\psi_{eq} - \cos(\psi_{eq} + \psi)) \tag{11}$$

and the moment exerted by the leaf spring assuming a constant curvature deformation is

$$M_{ls}(\psi) = \frac{EI}{a}(\pi - 2\alpha - 2(\psi_{eq} + \psi)) \tag{12}$$

It must be noted that it is essential for the expressions to be defined with respect to the equilibrium configuration for the dynamic analysis to be successfully carried out. Equation (4) is therefore re-expressed as a function of $\psi$ as

$$m\left(\left(\frac{dx_b}{d\psi}\right)^2 + \left(\frac{dx_t}{d\psi}\right)^2 + 2\left(\frac{dy}{d\psi}\right)^2\right)\ddot{\psi} + m\left(\left(\frac{dx_b}{d\psi}\right)\frac{d^2_{x_b}}{d\psi^2} + \left(\frac{dx_t}{d\psi}\right)\frac{d^2_{x_t}}{d\psi^2} + 2\left(\frac{dy}{d\psi}\right)\frac{d^2_y}{d\psi^2}\right)\dot{\psi}^2 + \left(2F_2(\psi)\left(\frac{dx_2}{d\psi}\right) - 2M_{ls}(\psi)\right) + 2M^* = 0 \tag{13}$$

which by reference to the equations defined above may be concisely expressed as

$$A(\psi)\ddot{\psi} + B(\psi)\dot{\psi}^2 + C(\psi) + 2M^* = 0 \tag{14}$$

This expression must be solved by numerical means. This is carried out by means of an explicit fourth-order Runge–Kutta process in MATLAB [14]. In the analysis, it is assumed that the structure is reconfigured from its high-energy stable equilibrium configuration $S_1$ by displacement control, past the unstable equilibrium, to the point at which positive stiffness is regained and it is legitimate to consider that the tape springs exert the constant moment $M^*$. It can be seen from Fig. 1(*a*) that this corresponds to an initial end rotation of 5.075 deg from horizontal. It must be recognized that this can result in some stored strain energy not being accounted for and consequently an underestimate of the jump height attained.

The solution of Eq. (14) enables the vertical accelerations of the two lumped masses $\ddot{x}_b$ and $\ddot{x}_t$ to be evaluated. By taking moments about the intersection point of the axes of symmetry in Fig. 4, the

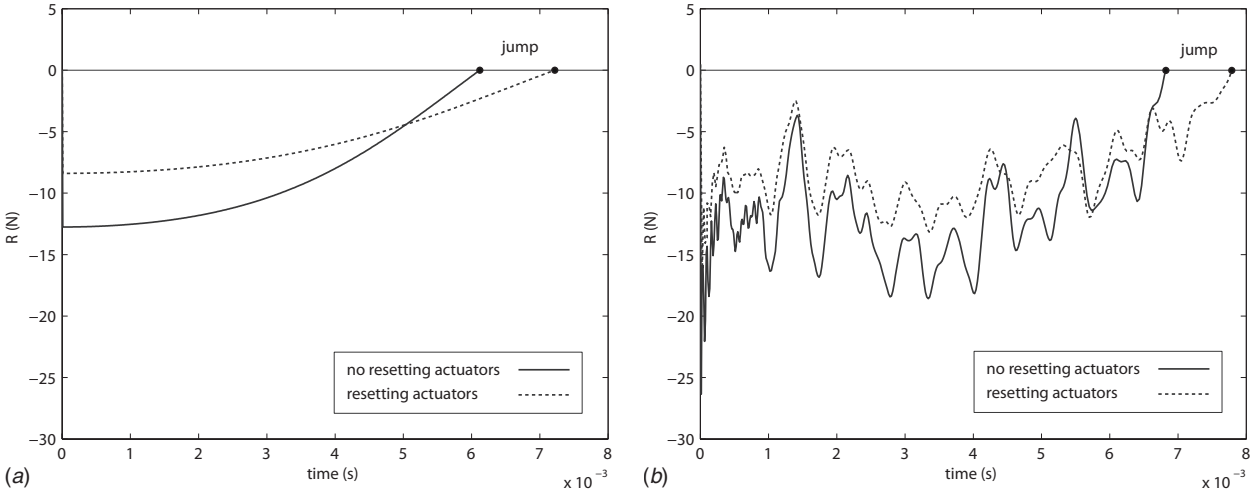


**Fig. 5 (*a*) Contact force *R* versus time evaluated using the simplified analytical model and (*b*) contact force *R* versus time evaluated using nonlinear dynamic FEA**

expression for the vertical force exerted by the structure at the point of contact between the foot and the ground $R$ as a function of time may be obtained as

$$R = -\left(\frac{b}{b+2L_2}\right)m(\ddot{x}_b + \ddot{x}_t) \tag{15}$$

The time when the bistable structure jumps during the transition is determined by the point at which this contact force becomes zero.

To determine the jump height that is achieved by the structure, the kinetic energy at the point of jump is evaluated. Some kinetic energy, however, does not contribute to the jump, resulting instead in oscillation of the structure itself. The kinetic energy that contributes to the structure jumping is that associated with the vertical velocities $\dot{x}_t$ and $\dot{x}_b$. The jumping kinetic energy $U_{\mathrm{KE}}$ of the structure, accounting for both sides, is therefore

$$U_{\mathrm{KE}} = 2 \times \tfrac{1}{2}m(\dot{x}_t^2 + \dot{x}_b^2) \tag{16}$$

By considering the conversion of this kinetic energy to potential energy, the jump height attained by the structure, evaluated by this simplified dynamic analysis is

$$s_{\mathrm{dy}} = \frac{U_{\mathrm{KE}}}{4mg} = \frac{(\dot{x}_t^2 + \dot{x}_b^2)}{4g} \tag{17}$$

in which $g$ is the acceleration due to gravity.

**3.5 Nonlinear Dynamic FEA.** One of the primary assumptions that was made in the simplified dynamic analysis in Sec. 3.4 was that the leaf spring always adopts a constant curvature along its length. This requirement for circular deformation is necessary in order to relate the displacements to the single variable $\psi$ to represent the dynamic behavior by means of the single differential equation Eq. (14). To account for the fact that the leaf spring may not deform in this fashion during the dynamic transition a nonlinear finite element analysis approach is used.

Two models of the jumping structure are considered. The first model is a refinement of the model shown in Fig. 4. The tape springs and the feet are modeled as rigid elements and the boundary conditions are as shown in the figure. The leaf spring is modeled with 40 Mindlin beam elements, however, all structural mass is still assumed to be lumped equally at the corners. Following a procedure similar to the one outlined in Sec. 3.1, the FEM is assembled in the configuration with straight leaf springs. It is then placed, by quasistatic displacement control, into the position when the corners are rotated 5.075 deg from the horizontal, corresponding to the configuration in which the tape springs have just buckled and exert a restoring moment $M^*$. This moment is applied to the two nodes on the vertical symmetry axis in the analysis. When the effect of reset actuation must be considered, the force $F_2$ as determined by Eq. (2) is applied to the relevant nodes.

To analyze the transition the structure is then released and a nonlinear dynamic analysis is carried out. The dynamic equation is solved using the second-order unconditionally stable Hilber–Hughes–Taylor (HHT) implicit-corrector scheme [15] to update the equilibrium equations before integration is carried out using the Newmark algorithm with automated time-stepping. The damping factor $\alpha$ in the HHT scheme must satisfy $0 \leq \alpha \leq \frac{1}{3}$, in which $\alpha = 0$ implies zero numerical damping. In the absence of any information concerning the expected damping, an intermediate value of $\alpha = 0.1$ was adopted. This assumption is adequate for initial design and could be modified in light of experimentation to account for any structural damping.

The vertical reaction force at the point of contact between the foot and the ground is monitored throughout the analysis. When it becomes zero, indicating a loss of contact and onset of jump, the kinetic energy resulting from the vertical velocities of the structure is evaluated. The attained jump height is calculated by converting this jumping energy into potential energy in a manner similar to that shown in Eq. (17).

The second model is based on the detailed representation of the structure that was used to determine the equilibrium configurations in Sec. 3.1. In this case the correct density is assigned to the elements representing the tape springs and leaf springs. Equal lumped masses of 11.25 g are placed at the centers of mass of the corner pieces to bring the combined structural mass to 70 g. When the effect of reset actuation is required, the force $F_2$ as determined by Eq. (2) is applied to the nodes at the locations of the actuator attachment points. Boundary conditions are as shown in Fig. 6 – the nodes corresponding to the points of contact between the structure and ground are free to translate horizontally; the nodes in the centers of the two tape springs are free to translate vertically.

The model is first displaced quasistatically from its high-energy (tape springs straight) equilibrium to the configuration in which the corner nodes are rotated 5.075 deg from the horizontal. A dynamic analysis of the transition is then carried out. In order to ensure the correct initial accelerations are present in the analysis, the dynamic response of the structure is computed for 1 s while being held in this starting configuration. Following this intermediate stage, the displacement control is released and the structure is allowed to transition dynamically. Once again the vertical reaction force at the point of contact between the foot and the ground

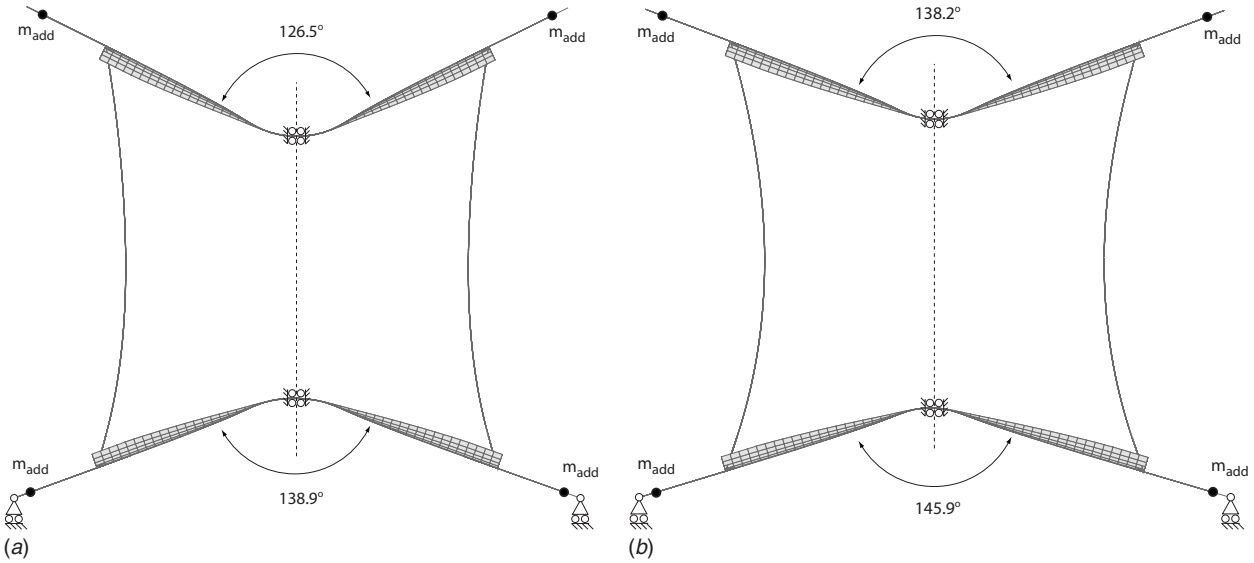


**Fig. 6 The dynamic FE model of the bistable jumping structure (*a*) neglecting resetting actuators and (*b*) including resetting actuators at the onset of jump showing the asymmetric transition path**

is monitored and when it becomes zero the onset of a jump is indicated. The jump height attained is also determined as described above.

## 4 Results

All the introduced analytical techniques are used to determine the jump height of the asymmetrically bistable structure resulting from the transition from the $S_1$ to $S_2$. Where the method permits, the dynamic transition time, from the point of release to the onset of jump is evaluated. In all cases the analysis is carried out for the specified design for the following two actuation cases: one in which the actuator behavior matches that of the NiTi springs in all respects and the other in which the force required to extend the actuator is zero. This is used to illustrate the desirability of unilateral actuation to transition bistable structures between their stable states.

The upper-bound energy-based analysis assuming perfect energy transfer, introduced in Sec. 3.3, is the simplest to carry out and yields jump heights of $s_{en}=0.556$ m when no energy is expended on extending opposing actuators and $s_{en}=0.319$ m when the extension of opposing actuators is included. It is not possible to estimate the frequency of dynamic transition using this approach.

The variation in contact force $R$ with time over the dynamic transition, evaluated using the simplified dynamic model with prescribed snap-through path, introduced in Sec. 3.4, is shown in Fig. 5(*a*). It was found that jump heights of 0.254 m and 0.146 m, and transition times of 0.0061 s and 0.0072 s were predicted when reset actuators were neglected and included, respectively. It can be seen that the effect of reset actuation is to reduce the jump height—as strain energy is absorbed that would otherwise be converted to potential energy—and to reduce the transition frequency.

**4.1 Dynamic FEA Results.** The dynamic FEA of the simplified model indicated that the jump heights are 0.193 m and 0.107 m and the transition times are 0.0064 s and 0.0074 s when reset actuators are neglected and included, respectively. Although the transition frequency predictions are not significantly altered when compared with the analytical model, the kinetic energy at onset of jump, and consequently the attained jump height, is reduced in both cases by approximately 25%. This indicates that it is essential to specify the correct transition path to ensure the correct energy transfer properties.

Similarly, the dynamic FEA of the detailed model indicated that the jump heights are 0.345 m and 0.222 m and the transition times are 0.0068 s and 0.0078 s when reset actuators are neglected and included, respectively. It can be seen that when the mass is correctly apportioned, the kinetic energy contributing to the structure jumping is substantially increased in both cases. The transition frequency is, however, not as significantly affected. In fact, for all the different analyses the transition time varies by up to 10% whereas the predicted jump height varies by up to 35%.

The variation in the force $R$ over the transition for this detailed model is shown in Fig. 5(*b*). In comparison with the variation plotted in Fig. 5(*a*) it can be seen that they are quantitatively similar. In both cases, the effect of including reset actuation is to reduce the peak reaction force, and the transition frequency. The structural configurations at the onset of jump are shown, both with and without reset actuation forces, in Fig. 6. In both cases it can be seen by inspection of the leaf spring shape, and by comparison of the top and bottom tape spring fold angles, that the assumption of the leaf springs deforming as circular arcs as assumed in the simplified analytical approach is incorrect.

**4.2 Physical Model.** In order to assess the above results, a physical model of the jumping bistable structure was fabricated and the jump height resulting from actuation $F_1$ and the transition $S_1$ to $S_2$ was measured. The video footage was taken of the jumps at 25 frames per second. Stills showing the structure at its maximum jump height are shown in Fig. 7. In order to capture the effect of zero reset actuation force while maintaining a comparable mass, the reset actuators were prestretched, so no energy was expended in extending them. The jump heights were measured to be 0.163 m and 0.145 m when the reset actuators were prestretched and not prestretched, respectively. To facilitate comparison, all the results from the transition analyses are compiled in Table 1.

On inspection it appears that the simplified analyses in which lumped masses are assumed provide the best predictions of the response of the physical model. This result is unexpected as it can be assumed that the nonlinear dynamic analysis would most closely represent the physical behavior. This may be explained by noting that, in performing the jump experiments, a number of additional sources of error in the form of energy sinks were made apparent. These include parasitic mass, for example the actuator power supply and friction between the feet and the ground resulting from the horizontal motion. None of these effects were incorporated in the analyses. It is believed that the extra energy ex-

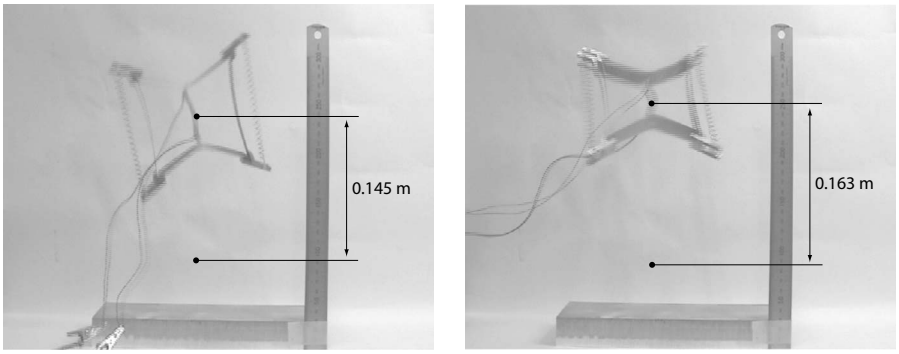


(*a*) (*b*)

**Fig. 7 (*a*) Bistable structure at the jump apogee, reset actuators pre-extended and (*b*) bistable structure at the jump apogee reset actuators not pre-extended**

pended as a result of the lumped mass assumption and transition path specification is equivalent to the energy lost in reality by the means described above.

## 5 Reset Analysis

Although this paper has concentrated on the high-frequency high-energy to low-energy transition, it is also necessary to ensure that the reset transition is possible with the chosen actuation scheme and actuators. The reset transition from the low-energy configuration $S_2$ to the high-energy configuration $S_1$ in which the tape springs are straightened is expected to occur at a much lower frequency than the transition in the opposite direction. The effect of the reset actuation $F_2$ is also to apply the same bending moment to both ends of the leaf springs and therefore cause a constant curvature. Consequently a quasistatic analysis in which the transition path is specified is considered sufficient to determine the reset actuation requirements.

To determine the minimum actuation force $F_2$ required to ensure completion of the reset transition, the geometry, snap-through path, and actuation forces illustrated in Fig. 4 are used. The conservation of energy results in the reduced form of Eq. (4) in which, due to the quasistatic nature of the transition, all accelerations are zero

$$2F_2 dx_2 + F_1 dx_1 + 2(M^* - M_{ls})d\psi = 0 \tag{18}$$

An analytical expression for the minimum reset actuation force requirement $F_2$ may be achieved by substituting Eqs. (6) and (7) into Eq. (18). The resulting minimum force requirement for the jumping bistable structure, determined from this expression, is plotted in Fig. 8 alongside the force that is applied by the NiTi spring actuators. It can be seen that the available actuation force is always greater than the required value throughout the transition, and therefore the actuators are suitable to carry out the reset. This reset capability is confirmed by the behavior of the physical model. Consequently, a full repeatable actuation cycle between the high-energy and low-energy states of an asymmetrically bistable structure has been demonstrated.

**Table 1 Kinetic energy corresponding to vertical velocities, jump heights attained, and transition times (where applicable) for bistable jumping structure analyses and experimental results**

| | Without reset actuation | | | With reset actuation | | |
|---|---|---|---|---|---|---|
| | Vert. KE (Nm) | *s* (m) | *t* (s) | Vert. KE (Nm) | *s* (m) | *t* (s) |
| Perfect transfer | 0.382 | 0.556 | — | 0.219 | 0.319 | — |
| Analytic model | 0.174 | 0.254 | 0.0061 | 0.100 | 0.146 | 0.0072 |
| Simplified FEA | 0.132 | 0.193 | 0.0064 | 0.074 | 0.107 | 0.0074 |
| Full FEA | 0.237 | 0.345 | 0.0068 | 0.153 | 0.222 | 0.0078 |
| Physical model | — | 0.163 | — | — | 0.145 | — |

## 6 Conclusions

In this paper actuated bistable structures have been analyzed with a focus on the dynamics of the transitions between the stable states. The complete repeated actuation of an asymmetrically bistable structure between the high-energy and low-energy stable states using existing technologies has been demonstrated with reference to the complete solution of a specific structure. This structure is itself a novel asymmetrically bistable adaptive device. The solution techniques may be readily extended to general cases. This is a vital step in the path to the incorporation of bistable structures into adaptive multistable systems.

The analysis techniques of increasing refinement have been developed and demonstrated, which have enabled the energy transfer during the transition from stored strain energy to kinetic energy to be determined. In the example considered this energy release as useful work manifests itself by the structure jumping. In all cases the effect of reset actuation which requires energy to extend has been incorporated into the analysis. This was carried out by representing actuators with nonlinear force-displacement functions. The techniques used, in order of increasing complexity, are as follows:

1. Upper-bound energy analysis

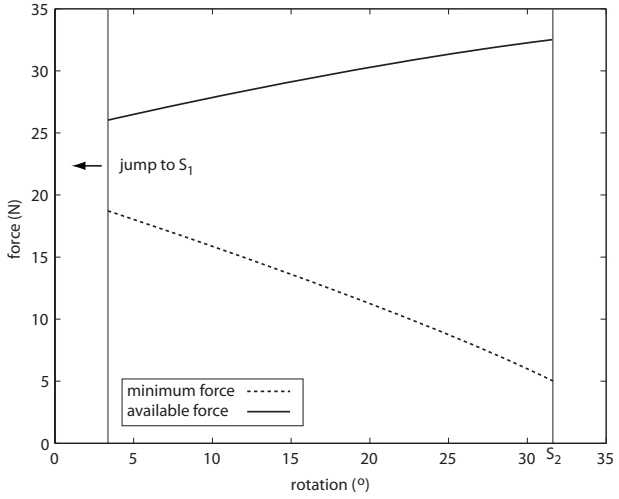


**Fig. 8 Minimum reset actuation force requirements and available reset actuation force over the transition from $S_2$ to $S_1$**

2. Analytic model with lumped mass and assumed transition path
3. FE model with lumped mass
4. FE model with correct mass distribution

It has been demonstrated that when asymmetrically bistable structures are actuated with low-frequency actuators, a high-frequency transition can occur due to the dynamic behavior of the structure itself. Also, the stored strain energy in the high-energy stable configuration may be released as useful work once the driving actuator has displaced the structure to the onset of instability. This ability to produce work at high-frequency, in excess of what is available with current actuator technologies, which have the required dimensions, is one of the key benefits of the technology. There is clearly a requirement for the development of suitable actuators, which require no energy to reset in order to maximize the work output.

The four analysis techniques itemized above all provided estimates of the efficiency of this transfer of strain energy to useful work, in this case resulting in the structure jumping. It was observed that the estimates of snap-through frequency were not substantially altered by increases in the model complexity. In fact, the qualitative behavior of the jumping structure during the transition was well captured by the simple analytical model. It was found, however, that it is important to model the mass distribution of the structure adequately as this has a substantial effect on the predicted energy transfer efficiency. The primary advantage of the simple upper-bound energy analysis is it may be carried out rapidly and is useful as a check for the more refined models. For design purposes, it also indicates the best performance that can be expected by providing a benchmark.

It was noted that if energy losses are present, for example due to friction, they must be adequately accounted for in the analysis. If they were included in the techniques above, it can be seen that the simplified analyses would substantially underestimate the kinetic energy at the onset of jump. This is clearly problem specific, and readily dealt with, for example by including additional terms in the energy equation Eq. (4). It should also be noted that structural damping could also play a role in the transitional behavior. This too must be considered on a case-to-case basis.

## Acknowledgment

The experimental component of this work was carried out at the University of Cambridge, with funding from the Cambridge-MIT Institute. Both institutions, in particular the technical staff at CUED, are gratefully acknowledged. Sergio Pellegrino, Paul Goulart, and Rafael Palacios are thanked for their valuable input. Fréderic Cugnon and Christopher Morton are thanked for the provision of SAMCEF and their technical insight. This work was motivated by conversations with Prof. Steven Dubowsky at MIT.

## References

[1] Chirikjian, G., 1994, "A Binary Paradigm for Robotic Manipulators," *Proceedings of the IEEE International Conference on Robotics and Automation*, Vol. 4, pp. 3063–3069.
[2] Howell, L., 2001, *Compliant Mechanisms*, Wiley, New York.
[3] Qiu, J., Lang, J. H., and Slocum, A. H., 2001, "A Centrally-Clamped Parallel-Beam Bistable MEMS Mechanism," *Proceedings of the 14th IEEE International Conference on MEMS*, pp. 353–356.
[4] Forterre, Y., Skotheim, J., Dumais, J., and Mahadevan, L., 2005, "How the Venus Flytrap Snaps," Nature (London), **433**, pp. 421–425.
[5] Santer, M. J., and Pellegrino, S., 2004, "An Asymmetrically-Bistable Monolithic Energy-Storing Structure," *Proceedings of the 45th AIAA/ASME/ASCE/AHS/ASC Structures, Structural Dynamics and Materials Conference*, AIAA Paper No. 2004-1527.
[6] Santer, M., and Pellegrino, S., 2008, "Compliant Multistable Structural Elements," Int. J. Solids Struct., **45**, pp. 6190–6204.
[7] Mattioni, F., Weaver, P. M., Potter, K. D., and Friswell, M. I., 2008, "Analysis of Thermally Induced Multistable Composites," Int. J. Solids Struct., **45**, pp. 657–675.
[8] Seffen, K., and Pellegrino, S., 1999, "Deployment Dynamics of Tape Springs," Proc. R. Soc. London, Ser. A, **455**, pp. 1003–1048.
[9] Samtech S.A., SAMCEF v12.0-03 Finite Element Package, Liege Science Park, Rue des Chasseurs-Ardennais, 8B-4031 Liège (Angleur), Belgium.
[10] Samtech S.A., 2007, SAMCEF v12.1 Documentation, Liege Science Park, Rue des Chasseurs-Ardennais, 8B-4031 Liège (Angleur), Belgium.
[11] Yee, J. C. H., Soykasap, Ö., and Pellegrino, S., 2004, "Carbon Fibre Reinforced Plastic Tape Springs," *Proceedings of the 45th AIAA/ASME/ASCE/AHS/ASC Structures, Structural Dynamics and Materials Conference*, AIAA Paper No. 2004-1819.
[12] Huber, J., Fleck, N., and Ashby, M., 1997, "The Selection of Mechanical Actuators Based on Performance Indices," Proc. R. Soc. London, Ser. A, **453**, pp. 2185–2205.
[13] Terentjev, E., Warner, M., Meyer, R., and Yamamoto, J., 1999, "Electromechanical Fredericks Effects in Nematic Gels," Phys. Rev. E, **60**, pp. 1872–1879.
[14] The MathWorks, MATLAB R2007b, 3 Apple Hill Drive, Natick, MA 01760-2098.
[15] Hilber, H., Hughes, T., and Taylor, R., 1977, "Improved Numerical Dissipation for Time Integration Algorithms in Structural Dynamics," Earthquake Eng. Struct. Dyn., **5**, pp. 283–292.